Molecular Motions of a Glycopeptide from Human Serum Transferrin Studied by ^{13}C Nuclear Magnetic Resonance

Jianyun Lu and Herman Van Halbeek
Complex Carbohydrate Research Center and Department of Chemistry, The University of Georgia, Athens, Georgia 30602 USA

ABSTRACT The molecular motions of a 21-amino-acid glycopeptide (Gp21) containing multiple glycoforms of an *N*-linked diantennary oligosaccharide were studied by two-dimensional ^1H-detected ^{13}C relaxation measurements at natural abundance. Gp21 was derived from human serum transferrin, its amino acid sequence is QQQHLFGSNVTDCSGNFCLFR, and its *N*-glycan structure is

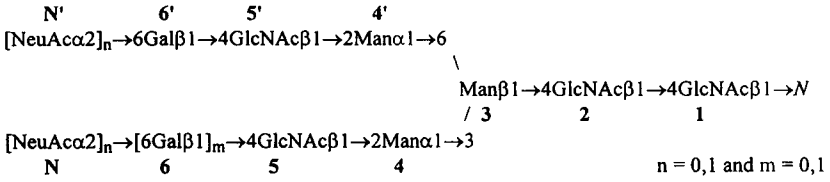

The measured longitudinal and transverse relaxation rate constants and the nuclear Overhauser enhancements for the methine carbons of Gp21 were analyzed by using the model-free approach to obtain information about the internal motions in the molecule. The calculated order parameters S^2 of the α carbons in both NH_2- and COOH-terminal segments of the peptide are smaller than those in the interior segment of the Gp21 peptide moiety, implying that the internal motions in the terminal segments are less restricted than in the interior segment. The average S^2 value is 0.72–0.91 for the glycosyl residues in the pentasaccharide core of Gp21, 0.58–0.59 for the interior GlcNAc-5,5′ residues in the two branches, and 0.35–0.51 for the terminal GlcNAc-5, Gal-6,6′, and NeuAcN,N′ residues in the two branches, indicating that the internal motions in the glycan core are more restricted than in the two branches.

INTRODUCTION

Conformational flexibility of *N*-linked oligosaccharides in aqueous solution is of interest to glycobiologists from both structural and biological points of view (Homans et al., 1987; Carver, 1991; Van Halbeek, 1994). This flexibility has been held responsible for the fact that very few of these oligosaccharides in the free state have been crystallized so far (Meyer, 1990). Furthermore, the *N*-linked oligosaccharides are generally not resolved in the x-ray crystal structure of glycoproteins (if at all available), due to the motional disorder of the carbohydrate residues; typically, only the first one or two GlcNAc residues are discernible in electron density maps (Woods et al., 1994). One approach to characterize the oligosaccharide's flexibility is computer simulation of the dynamics of the flexible molecule. A number of molecular dynamics (MD) simulations using different force fields (Woods et al., 1994; Rutherford et al., 1993; Lommerse et al., 1995; Balaji et al., 1993; Dauchez et al., 1992; Homans, 1990) have been applied to different oligosaccharide systems.

The experimental approach to gain insight into the conformational flexibility of the *N*-glycans requires the use of methods that are capable of characterizing these motions, such as fluorescence (Lakowicz, 1986) and nuclear magnetic resonance (NMR) spectroscopies (Ernst, 1987). Among different experimental techniques, NMR is uniquely capable of characterizing the conformational change of a molecule in solution at the atomic level over time scales ranging from picoseconds to hours (Brüschweiler, 1994). Slow exchange between two or more chemically distinct conformations can be investigated by using chemical shift measurements, line-shape analysis, T_2 measurements, and saturation transfer experiments. Fast exchange among locally favorable conformations or conformational substrates separated by potential energy barriers that are smaller than or comparable to thermal energies, due to the internal and overall motions of the molecule, can be investigated by relaxation rate measurements. The ^{13}C relaxation measurements are, in particular, suitable for such studies, because the relaxation of protonated ^{13}C nuclei at natural abundance is dominated by the dipolar interaction with the attached

Received for publication 17 May 1996 and in final form 23 September 1996.

Address reprint requests to Dr. Herman Van Halbeek, Rega Institute, Department of Medicinal Chemistry, Katholieke Universiteit Leuven, Minderbroedersstraat 10, B-3000 Leuven, Belgium. Tel.: 32-16-337389; Fax: 32-16-337340; E-mail: herman.vanhalbeek@rega.kuleuven.ac.be.

Dr. Lu's current address: Washington University School of Medicine, 660 South Euclid, Campus Box 8051, St. Louis, MO 63110.

0006-3495/97/01/470/12 $2.00

protons (Abragam, 1961; Peng and Wagner, 1994), leading to a relatively straightforward interpretation in terms of molecular motion. However, until recently, the application of ^{13}C relaxation measurements to the study of carbohydrate dynamics has been hindered by the low ^{13}C natural abundance and inherent lack of sensitivity. The development of two-dimensional proton-detected heteronuclear NMR techniques (Sklenar et al., 1987; Kay et al., 1987) enables heteronuclei to be indirectly monitored with increased sensitivity; at the same time, the spectral resolution increases over that in a one-dimensional ^{13}C spectrum. Thus, many studies of heteronuclear relaxation in proteins with ^{15}N enrichment (Kay et al., 1989; Clore et al., 1990; Barbato et al., 1992) and proteins at natural ^{13}C isotopic abundance (Palmer et al., 1991) have been performed recently. A number of ^{13}C relaxation studies on complex oligosaccharide systems at natural isotopic abundance have also been reported; these include the carbohydrate headgroup of ganglioside GD1a anchored in a micelle in aqueous solution (Poppe et al., 1994) and the oligomannose glycan of ribonuclease B (RNAse B) covalently linked to the parent protein (Rutherford et al., 1993).

Previously, we have reported the complete ^{1}H and ^{13}C resonance assignments of a 21-amino-acid glycopeptide (Gp21) prepared from human serum transferrin (Lu and Van Halbeek, 1996). Gp21 consists of a peptide fragment of 2.5 kDa, with a single glycosylation site to which a diantennary oligosaccharide is attached:

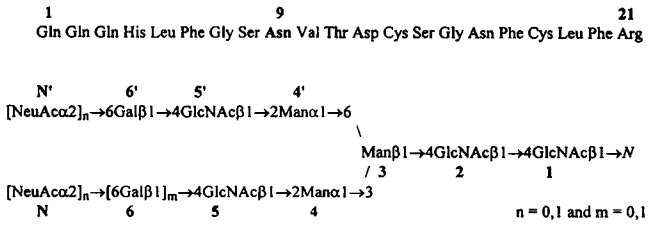

Gp21 can serve as a good model for the investigation of oligosaccharide dynamics, as it mimics a *N*-linked diantennary oligosaccharide in covalent association with a protein. In the present work, two-dimensional proton-detected ^{13}C NMR spectroscopy has been used to measure the longitudinal and transverse relaxation rate constants and the $[^{1}H]^{13}C$ nuclear Overhauser effect (NOE) enhancements for the methine ^{13}C resonances of Gp21 at natural isotopic abundance.

In the literature, different approaches (Kowalewski, 1989) have been applied to interpret the relaxation parameters for complex carbohydrates in terms of molecular motions. Some studies have used approaches that require an explicit dynamic model (Ejchart and Dabrowski, 1992), whereas others have used an approach that does not require an explicit dynamic model (Rutherford et al., 1993; Poppe et al., 1994; Bagley et al., 1992; Mäler et al., 1996). It has been generally recognized that the model-free approach (Lipari and Szabo, 1982a) is the preferred choice to extract dynamic information from a limited number of relaxation parameters. In this work, we have applied the model-free approach to characterize the dynamics of Gp21. The two model-independent quantities, i.e., the generalized order parameter (S^2) and the effective correlation time (τ_e), which are the measure of the spatial restriction and the rate of the motion, respectively, have been extracted for the methine ^{13}C resonances of Gp21.

MATERIALS AND METHODS

Sample preparation

The isolation and purification of Gp21 from human serum transferrin have been reported previously (Lu and Van Halbeek, 1996). The Gp21 sample (15.0 mg, derived from human serum transferrin lot 72H9303, Sigma Chemical Co., St. Louis, MO) was twice subjected to deuterium exchange in D_2O (99.9%; Cambridge Isotope Laboratories, Andover, MA) with 100 mM NH_4HCO_3 (pH 8.0) and then dissolved in 500 μl D_2O (99.96%). The solution was titrated with 0.1 M DCl to reach pH 6.1 and then sealed for NMR studies.

NMR Spectroscopy

All experiments were carried out on a Bruker DRX600 spectrometer equipped with three channels and xyz-pulsed-field gradients. The ^{13}C relaxation experiments included the measurements of the longitudinal relaxation rates R_1 (Kay et al., 1992), the transverse relaxation rates R_2 (Kay et al., 1992), and the steady-state heteronuclear NOE enhancements η (Peng and Wagner, 1994; Barbato et al., 1992). As slightly different conditions (20°C and pH 6.1) from those reported previously (Lu and Van Halbeek, 1996) for the ^{13}C resonance assignment were used in all of the ^{13}C relaxation experiments, heteronuclear single-quantum correlation (HSQC) (Bodenhausen and Ruben, 1980) and gradient-enhanced HSQC-total correlation spectroscopy (TOCSY) (Bax and Pochapsky, 1992) experiments were performed to verify the ^{13}C chemical shifts of Gp21. All spectra were acquired in a pure phase manner by using the time-proportional phase incrementation (TPPI) method (Marion and Wüthrich, 1983) in t_1 and quadrature detection in t_2; 1024 data points were recorded with oversampling and digital filtering (Delsuc and Lallemand, 1986) in t_2 and 200 real points were recorded in t_1. The spectra were acquired with a spectral width of 1200 Hz in the F_2 domain and 6791 Hz in the F_1 domain; the ^{1}H carrier was set at 4.28 ppm and the ^{13}C carrier at 67.73 ppm. The ^{1}H chemical shifts were referenced to internal acetone (2.225 ppm) and the ^{13}C chemical shifts were referenced indirectly to sodium 4,4-dimethyl-4-silapentane-1-sulfonate (DSS) with use of the ^{1}H frequency of internal acetone (Lu and Van Halbeek, 1996). For the R_1, R_2 and η measurements, 64 scans were acquired per t_1 increment with a 4.3-s inter-scan delay and 0.4-s acquisition time; for the HSQC and HSQC-TOCSY experiments, 32 and 256 scans were acquired per t_1 increment, respectively, with a 1.5-s inter-scan delay and 0.4-s acquisition time. The refocusing delay ($1/2J$) was set at 3.0 ms in all experiments except for HSQC-TOCSY, for which it was set at 3.3 ms. In the HSQC-TOCSY experiment, the MLEV17 sequence (Bax and Davis, 1985) flanked by 1.5-ms trim pulses was used for the isotropic mixing with a duration of 40 ms. The ^{13}C decoupling during acquisition was achieved using the GARP-1 sequence (Shaka et al., 1985) in all experiments. For R_1 measurements, seven spectra were recorded with relaxation delays of 20, 40, 80, 120, 160, 321, and 481 ms, respectively. For R_2 measurements, seven spectra were recorded with relaxation delays of 11, 22, 44, 66, 88, 154, and 198 ms, respectively. For η measurements, three spectra with ^{1}H pre-irradiation were recorded under the same conditions, and another two spectra without ^{1}H pre-irradiation were recorded under the same conditions. Data were processed on an IRIS 4D/220GTX workstation (Silicon Graphics, Mountain View, CA) using

Felix 2.30 (Biosym Technologies, San Diego, CA). The data were zero-filled in the F_1 domain and multiplied with a 90° shifted squared sinebell function in the F_1 domain and a Gaussian line-broadening function (lb = −1.5 Hz, gb = 0.05) in the F_2 domain before Fourier transformation. The resulting spectra were 1024 × 1024 matrices. Baseline correction was applied to all spectra.

Relaxation parameter (R_1, R_2, and η) calculations

The longitudinal and transverse relaxation rates (R_1 and R_2, respectively) and the steady-state NOE (η) of the methine ^{13}C resonances were calculated from the cross-peak heights measured in the two-dimensional spectra. The data for both relaxation rates were analyzed by two-parameter non-linear least-squared fit of a single exponential function (Kay et al., 1992):

$$I(t) = I_0 \exp(-R_n t), \tag{1}$$

in which $I(t)$ is the measured peak height, t is the relaxation delay, I_0 is the calculated peak height at zero relaxation delay, and R_n (n = 1 and 2) are the calculated longitudinal and transverse relaxation rates, respectively. The steady-state NOE was calculated by using equation

$$\eta = \frac{I_{sat}}{I_{unsat}} - 1, \tag{2}$$

in which I_{sat} and I_{unsat} are the peak heights measured in the spectra recorded with and without ^1H pre-irradiation, respectively.

Model-independent parameter (S^2, τ_e) calculations

The relaxation of protonated ^{13}C nuclei at natural abundance is mediated primarily by the dipolar interaction with the attached protons (Abragam, 1961). Thus, the calculated relaxation parameters have the following relationships with the spectral density functions:

$$R_1 = \frac{D_{CH}^2}{4}[J(\omega_H - \omega_C) + 3J(\omega_C) + 6J(\omega_H + \omega_C)] \tag{3}$$

$$R_2 = \frac{D_{CH}^2}{8}[4J(0) + J(\omega_H - \omega_C) + 3J(\omega_C) + 6J(\omega_H) + 6J(\omega_H + \omega_C)] \tag{4}$$

$$\eta = \frac{\gamma_H[6J(\omega_H + \omega_C) - J(\omega_H - \omega_C)]}{\gamma_C[J(\omega_H - \omega_C) + 3J(\omega_C) + 6J(\omega_H + \omega_C)]}, \tag{5}$$

in which

$$D_{CH} = \frac{h}{2\pi}(\gamma_H \gamma_C r_{CH}^{-3})\frac{\mu_0}{4\pi}, \tag{6}$$

where h is Planck's constant (6.626×10^{-34} J s), r_{CH} is the carbon-hydrogen bond length (1.09×10^{-10} m), μ_0 is the permeability of free space ($4\pi \times 10^{-7}$ T m A^{-1}), γ_H and γ_C are the ^1H (2.6752×10^8 s^{-1} T^{-1}) and ^{13}C (6.728×10^7 s^{-1} T^{-1}) gyromagnetic ratios, respectively, ω_H and ω_C are the ^1H ($2\pi \times 600.13$ MHz) and ^{13}C ($2\pi \times 150.91$ MHz) Larmor frequencies, respectively, and $J(\omega)$ is the spectral density function. In the model-free approach (Lipari and Szabo, 1982a), the spectral density function for the molecular motions is expressed by

$$J(\omega) = \frac{2}{5}\left(\frac{S^2\tau_m}{1 + (\omega\tau_m)^2} + \frac{(1 - S^2)\tau}{1 + (\omega\tau)^2}\right), \tag{7}$$

in which $\tau^{-1} = \tau_m^{-1} + \tau_e^{-1}$, τ_m is the overall rotational correlation time of the molecule, S^2 is the generalized order parameter, and τ_e is the effective correlation time.

The model-independent parameters S^2 and τ_e for each of the methine ^{13}C resonances were calculated from the relaxation parameters by performing numerical minimization, with constraints $0 \le S^2 \le 1$ and $0 \le \tau_e \le \tau_m$, of a target function $f(S^2,\tau_e)$, which is expressed by

$$f(S^2, \tau_e) = \frac{(R_1 - R_1^{exp})^2}{\sigma_1^2} + \frac{(R_2 - R_2^{exp})^2}{\sigma_2^2} + \frac{(\eta - \eta^{exp})^2}{\sigma_3^2}, \tag{8}$$

in which R_1, R_2, and η are the values calculated with Eqs. 3, 4, and 5; R_1^{exp}, R_2^{exp}, and η^{exp} are the experimental values of the relaxation parameters; σ_1, σ_2 and σ_3 are the standard errors of the relaxation parameters. The numerical minimization was carried out by using the downhill simplex method (Press et al., 1992) because it does not require the derivative of the target function. The value for τ_m was first calculated from the average of the R_2/R_1 ratios (Kay et al., 1989; Clore et al., 1990; Palmer et al., 1991) by performing numerical minimization of the target function $g(\tau_m)$, which is expressed by

$$g(\tau_m) = \frac{R_2}{R_1} = \frac{2}{1}\left(\frac{4J'(0) + J'(\omega_H - \omega_C) + 3J'(\omega_C) + 6J'(\omega_H) + 6J'(\omega_H + \omega_C)}{J'(\omega_H - \omega_C) + 3J'(\omega_C) + 6J'(\omega_H + \omega_C)}\right), \tag{9}$$

in which $J'(\omega)$ is the simplified spectral density function of the form

$$J'(\omega) = \frac{S^2\tau_m}{1 + (\omega\tau_m)^2} \tag{10}$$

Later, the τ_m value was optimized globally by minimizing, with a bisection method, the sum of the target function f_i:

$$\chi^2 = \sum_i f_i(S_i^2, \tau_{ei}, \tau_m), \tag{11}$$

in which f_i has the form of Eq. 8, and i is the index of the ^{13}C resonances the R_2/R_1 ratios of which are within one standard deviation of the mean value.

The uncertainties in the model-independent parameters were estimated by Monte Carlo simulations (Press et al., 1992). The deviations of the relaxation parameters were assumed to have a Gaussian distribution (Palmer et al., 1991) with the experimental values and the standard deviations of the relaxation parameters taken as the means and the standard deviations of the distribution curves. Five hundred simulated data sets for each ^{13}C resonance were generated and then analyzed, and the averages and standard deviations of the simulated model-independent parameters were determined. These standard deviations are reported as those of the optimized model-independent parameters.

The R_1 and R_2 values were calculated using SigmaPlot software (Jandel Scientific, San Rafael, CA) on an IBM-compatible PC. The S^2, τ_e, and τ_m values were calculated using in-house modified versions of the commercial C-programs (Press et al., 1992) on an IBM-compatible PC.

RESULTS AND DISCUSSION

^{13}C resonance assignment

The complete ^{13}C resonance assignment of Gp21 has been reported previously (Lu and Van Halbeek, 1996); in that study, the ^{13}C chemical shifts were measured at 25°C and pH 4.6. However, it was found that the heteronuclear experiments with the sample at pH 6.1 afforded spectra with a

slightly better signal-to-noise ratio than those at pH 4.6. In addition, lowering the temperature by 5°C avoided interference of the water resonance with the ^{1}H signals of Man-3 C1 and Asn-9 C$^\alpha$. Therefore, all NMR experiments in this study were conducted on a 5.6 mM Gp21 sample at pH 6.1 and 20°C. The methine ^{13}C resonance assignments at 20°C and pH 6.1 are indicated in Fig. 1. The assignments have been verified by homonuclear and heteronuclear correlation experiments, including HSQC-TOCSY (data not shown). For virtually all methine ^{13}C resonances of Gp21, the ^{13}C chemical shifts differed no more than 0.2 ppm from the values reported previously. Only the ^{13}C chemical shifts of the peptide fragment Gln-1 to His-4 differed by up to 2 ppm.

For the peptide fragment, the resonances of Phe-6 and Phe-17 were found superimposed on each other; the same applied to those of pGlu-1 and Ser-14, as shown in Fig. 1. The intensities measured for the two C$^\alpha$ signals were divided equally between constituting residues. The resonances of Ser-8 and one of the two Gln-2 (namely, Gln-2 when pGlu was at the peptide's NH_2 terminus) were partially overlapped, and only the stronger intensity signal of Ser-8 could be measured accurately. The methylene C$^\alpha$ resonances of the two Gly residues (Gly-7 and Gly-15) and the rest of the methylene carbon resonances of Gp21 were suppressed by the insensitive nuclei enhanced by polarization transfer (INEPT) and could hardly be observed in these relaxation experiments. For the carbohydrate moiety, the chemical shifts of the ^{13}C resonances of the GlcNAc-5,5′, Gal-6,6′, and NeuAc-N,N′ residues in both branches were pairwise degenerate, and so were those of the C3 and C4 of Man-4 and Man-4′. The presence of NeuAc affected the chemical shifts of a number of ^{13}C resonances in the branches, including the C1 and C5 of Gal-6,6′ and C4 of GlcNAc-5,5′. These resonances in the sialylated and non-sialylated branches were sufficiently resolved for intensity measurement. There are three severe overlap regions marked by A, B, and C in Fig. 1. Region A contains the C3 signals of GlcNAc-1, -2, -5, and -5′, the C3 signal of Gal-6,6′, and the C6 signal of NeuAc-N,N′; nonetheless, the intensities of the C3 signal of Gal-6,6′ and the C3 signal of GlcNAc-1 could still be measured accurately. Region B contains the C5 signals of Man-3, GlcNAc-2, -5, and -5′, and only the intensity of the Man-3 C5 signal could be measured accurately. Region C contains the C2 signals of GlcNAc-2, -5, and -5′, and only the intensity of the C2 signal of GlcNAc-2 could be measured accurately.

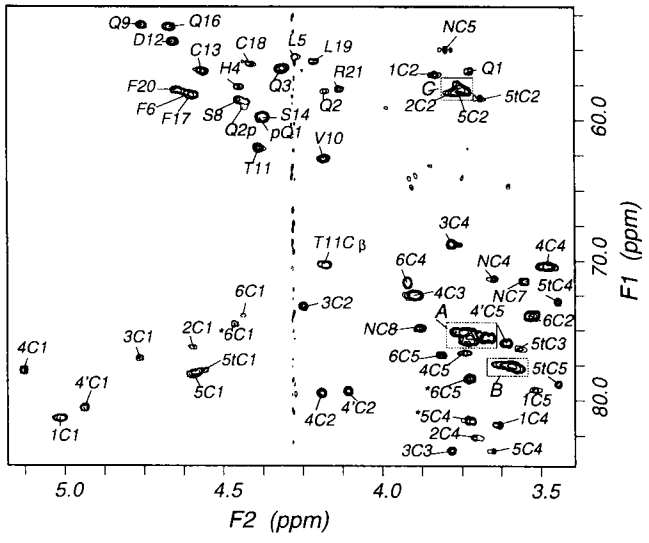

FIGURE 1 HSQC spectrum of Gp21 used for the longitudinal relaxation rate measurements recorded with 20-ms relaxation delay. The peaks drawn in dotted lines at the lower left corner are negative due to the folding of the signals outside the spectral width in the F_1 domain. The methine carbon assignments for the amino acid and sugar residues are indicated differently. For the former, the one-letter code is used, followed by the sequence number. For the latter, the numbers before and after C represent the residue and the carbon position in the ring, respectively. The ^{13}C chemical shifts of the GlcNAc, Gal and NeuAc residues in the α(1→3) and α(1→6) branches are degenerate, and so are those of the C3 and C4 of Man-4 and Man-4′. Therefore, only the assignments for the α(1→3) branch are indicated. The asterisk indicates the different chemical shift of the pertinent methine carbon affected by the absence of NeuAc in the branch. Label 5t represents the terminal GlcNAc-5 in two of the five glycoforms found in this sample. See the text for the detailed description of the three regions (A, B, and C) with severe overlap.

Calculation and evaluation of relaxation parameters

The longitudinal and transverse relaxation rate constants and the NOE enhancements for Gp21 were calculated from the measured peak heights and root-mean-square baseline noise (Kay et al., 1989; Palmer et al., 1991) with Eqs. 1 and 2; the resulting R_1, R_2, and η values are listed in Tables 1 and 2 for the peptide and the carbohydrate moieties, respectively. Expanded spectra acquired with different relaxation delays for the measurements of longitudinal and transverse relaxation rates are shown in Figs. 2 and 3, respectively. The longitudinal and transverse relaxation decay curves for the C$^\alpha$ of Val-10, the C2 of Man-4, and the C4 of NeuAc-N,N′ are shown in Fig. 4 together with the optimized fits of the peak intensities to Eq. 1. It is evident that both the longitudinal and transverse relaxation decay curves can be fit with a single exponential function (Kay et al., 1992).

The R_1 values for most of the methine ^{13}C resonances (see Tables 1 and 2) are very similar and within the range of 2.0–3.0 s^{-1}, indicating that the Gp21 molecule is tumbling isotropically in solution (Kowalewski, 1989; Bagley et al., 1992). It is known from theoretical calculations (Harris, 1983) and experimental evidence (Kay et al., 1989) that the R_1 and R_2 values are sensitive to different motional frequencies. The R_1 relaxation rates provide information about motional properties with a frequency in the range of 10^8-10^{12} s^{-1}, whereas the R_2 relaxation rates, in addition to depending on motions occurring at these high frequencies, are also sensitive to dynamics on the micro- and millisecond time scale. Therefore, by measuring both relaxation parameters, it is possible to obtain dynamic information over a large motional regime. A large variability of the R_2 values

TABLE 1 Relaxation parameters for the methine ^{13}C resonances of the Gp21 peptide fragment measured at 20°C and pH 6.1

Residue*	R_1 (s^{-1})#	R_2 (s^{-1})	η§	R_2/R_1¶
Backbone $^{13}C^{\alpha}$				
Gln-1	0.19 ± 0.01	4.1 ± 0.5	1.1 ± 1.1	21 ± 3
pGlu-1	2.0 ± 0.1	4.9 ± 0.1	0.69 ± 0.09	2.4 ± 0.1
Gln-2	2.5 ± 0.1	4.3 ± 0.8	1.0 ± 0.6	1.7 ± 0.3
	2.1 ± 0.2	11 ± 1	0.48 ± 0.28	5.5 ± 0.8
Gln-3	2.4 ± 0.1	2.5 ± 0.3	0.95 ± 0.07	1.0 ± 0.1
His-4	1.9 ± 0.2	7.6 ± 0.8	0.53 ± 0.32	4.0 ± 0.7
Leu-5	2.8 ± 0.4	3.4 ± 1.5	0.11 ± 0.42	1.2 ± 0.6
Phe-6	3.0 ± 0.2	7.2 ± 0.9	0.85 ± 0.69	2.4 ± 0.3
Ser-8	2.5 ± 0.3	9.0 ± 0.4	0.44 ± 0.19	3.7 ± 0.5
Asn-9	2.8 ± 0.2	12 ± 2	0.90 ± 0.19	4.2 ± 0.6
Val-10	2.3 ± 0.1	6.8 ± 0.5	0.37 ± 0.33	2.9 ± 0.3
Thr-11	2.6 ± 0.2	7.8 ± 0.8	0.33 ± 0.26	3.0 ± 0.4
Asp-12	2.8 ± 0.1	9.2 ± 0.8	0.53 ± 0.20	3.4 ± 0.3
Cys-13	2.7 ± 0.1	7.2 ± 0.7	0.66 ± 0.16	2.7 ± 0.3
Ser-14	2.0 ± 0.1	4.9 ± 0.1	0.69 ± 0.09	2.4 ± 0.1
Asn-16	2.7 ± 0.2	6.3 ± 0.6	0.85 ± 0.28	2.3 ± 0.3
Phe-17	3.0 ± 0.2	7.2 ± 0.9	0.85 ± 0.69	2.4 ± 0.3
Cys-18	3.6 ± 0.2	6.3 ± 0.5	0.15 ± 0.12	1.7 ± 0.2
Leu-19	3.3 ± 0.4	6.6 ± 0.9	0.33 ± 0.33	2.0 ± 0.4
Phe-20	2.8 ± 0.2	5.4 ± 0.7	0.70 ± 0.25	1.9 ± 0.3
Arg-21	2.6 ± 0.2	9.9 ± 1.2	0.73 ± 0.39	3.8 ± 0.5
Side-chain methine ^{13}C‖				
Thr-11 $^{13}C^{\beta}$	3.0 ± 0.2	7.4 ± 0.4	0.14 ± 0.16	2.5 ± 0.2

*Each of the two pairs of residues, pGlu-1 and Ser-14 as well as Phe-6 and Phe-17, shares the same data set with the other because their signals are superimposed. The two Gly residues are not included in this table because Gly does not contain a methine ^{13}C. The second data set for Gln-2 is due to the presence of pGlu at the NH_2 terminus in a portion of the Gp21 molecules.

#The limit associated with the R_1 and R_2 values (in the next column) is the standard error.

§The mean and standard deviation of six η values calculated from three I_{sat} and two I_{unsat} values.

¶The deviation is calculated according to the random error propagation rule.

‖Relaxation rates for other amino acid side-chain methine carbons, including the β-carbon of Val-10 and the γ-carbons of the two Leu residues, were not measured because their signals are outside the chosen spectral width.

ranging from 2.5 ± 0.3 s^{-1} for the Gln-3 C^{α} to 13 ± 2 s^{-1} for the Man-3 C5 was observed for Gp21, as shown in Tables 1 and 2. In particular, the R_2 value for Asn-9 C^{α} is the largest among those measured for the peptide fragment, and those for Ser-8, Asp-12, and Arg-21 C^{α} are also larger than for the rest of the peptide fragment. For the carbohydrate moiety, the R_2 values for C5 of the three Man residues and C1 of GlcNAc-1 are over 11.0 s^{-1}; these values are the largest among those for the carbohydrate moiety. The average R_2 values for GlcNAc-2 and Man-3 in the pentasaccharide core are significantly higher than those for the residues in the branches, indicating that the dynamics properties of the sugar residues in the core and the branches may be different from each other. Similar observations were reported (Wyss et al., 1995) for the oligomannose glycan chain covalently linked to the adhesion domain of human CD2; those conclusions were based on ^{13}C line width data, a parameter that is closely related to R_2 (line width $\Delta\omega = R_2/\pi$).

The $[^1H]^{13}C$ NOE enhancement, with a theoretical maximal value of 1.99 in the extreme narrowing limit, is also sensitive to internal motion (Neuhaus and Williamson, 1989), which is on the pico- and nanosecond time scale as mentioned above. Each η value listed in Tables 1 and 2 is the average of six values calculated from the combinations of the three I_{sat} and two I_{unsat} values for each of the methine carbons of Gp21. Due to the low signal-to-noise ratios in the spectra recorded without proton pre-irradiation, some η values have a large standard deviation. Nonetheless, most of the η values are rather small relative to the maximal value of 1.99, indicating that under the chosen experimental conditions the Gp21 molecule is tumbling slowly relative to the extreme narrowing limit.

Calculation of model-independent parameters

The relaxation parameters were analyzed by using the model-free approach with a spectral density function expressed by Eq. 7, in which it was assumed that the molecule tumbles isotropically in solution. This assumption is justified by the similarity in the R_1 values of Gp21 mentioned above and by the results of a study on a similar oligosaccharide system (Poppe et al., 1994). The values of R_2/R_1 for the methine ^{13}C resonances, listed in Tables 1 and 2, were used to derive an initial value of the overall rotational correlation time of Gp21 by minimizing the target function $g(\tau_m)$ in Eq. 9. The mean R_2/R_1 ratio is 3.5 ± 1.0 with a span ranging from 1.0 for Gln-3 to 21 for Gln-1. The values at more than one standard deviation off the mean were excluded from being used for the τ_m calculation, because internal motions made a significant contribution to the R_1 in case of a very small R_2/R_1 ratio, and chemical or conformational exchange (with a low frequency) processes made a significant contribution to the R_2 in case of a very large R_2/R_1 ratio (Clore et al., 1990). The R_2/R_1 ratios for the remaining residues (with a mean of 3.2 ± 0.9) were then fitted simultaneously by optimizing τ_m as the only free parameter with Eq. 9. The optimized τ_m value was 1.96 ns; this value was used as the initial value of the overall rotational correlation time for the calculation of the model-independent parameters.

The model-independent parameters S^2 and τ_e for Gp21 were calculated from the relaxation parameters by using the procedure described in Materials and Methods; the resulting S^2 and τ_e values are listed in Tables 3 and 4 for the peptide and the carbohydrate moieties, respectively. The τ_m value that was globally optimized by using Eq. 11 is 2.35 ± 0.01 ns. The small standard deviations associated with most of the generalized order parameters in Tables 3 and 4 calculated by Monte Carlo simulations indicate that the calculated S^2 values are reliable with at least 95% confidence limit except for a few cases. The S^2 value for Gln-1 C^{α} is not reliable because the minimization failed to reach convergence. The S^2 value for the resonances the peak heights of

TABLE 2 Relaxation parameters for methine ^{13}C resonances of the Gp21 carbohydrate moiety measured at 20°C and pH 6.1

Residue*	Parameter#	C1	C2	C3	C4	C5	Average§
GlcNAc-1	R_1 (s^{-1})	2.3 ± 0.2	2.3 ± 0.2	2.6 ± 0.4	2.6 ± 0.4	2.6 ± 0.3	$2.5 \pm 0.2^{1-5}$
	R_2 (s^{-1})	9.0 ± 0.5	9.0 ± 0.8	8.6 ± 1.0	10 ± 1	7.2 ± 0.8	$8.8 \pm 1.0^{1-5}$
	η	0.29 ± 0.12	0.18 ± 0.14	0.55 ± 0.20	0.57 ± 0.12	0.20 ± 0.14	$0.36 \pm 0.19^{1-5}$
	R_2/R_1	3.9 ± 0.3	3.9 ± 0.5	3.3 ± 0.6	4.0 ± 0.7	2.8 ± 0.4	$3.6 \pm 0.5^{1-5}$
GlcNAc-2	R_1 (s^{-1})	2.2 ± 0.2	2.3 ± 0.3	2.4 ± 0.2	2.3 ± 0.3	2.5 ± 0.2	$2.3 \pm 0.1^{1-4}$
	R_2 (s^{-1})	11 ± 1	10 ± 1	9.6 ± 1.7	9.8 ± 0.6	9.6 ± 0.6	$10 \pm 0.6^{1-4}$
	η	0.21 ± 0.06	0.36 ± 0.16	0.54 ± 0.20	0.76 ± 0.35	0.63 ± 0.21	$0.47 \pm 0.24^{1-4}$
	R_2/R_1	5.1 ± 0.8	4.5 ± 0.6	4.0 ± 0.7	4.2 ± 0.6	3.8 ± 0.4	$4.5 \pm 0.5^{1-4}$
Man-3	R_1 (s^{-1})	2.0 ± 0.2	2.2 ± 0.1	3.0 ± 0.2	2.6 ± 0.3	2.9 ± 0.2	$2.5 \pm 0.4^{1-5}$
	R_2 (s^{-1})	9.1 ± 0.9	11 ± 1	9.9 ± 1.1	9.6 ± 0.6	13 ± 2	$11 \pm 1.6^{1-5}$
	η	0.10 ± 0.15	0.25 ± 0.09	0.47 ± 0.15	0.26 ± 0.13	0.94 ± 0.70	$0.27 \pm 0.15^{1-4}$
	R_2/R_1	4.5 ± 0.6	5.1 ± 0.4	3.3 ± 0.4	3.7 ± 0.5	4.4 ± 0.8	$4.2 \pm 0.7^{1-5}$
Man-4	R_1 (s^{-1})	3.0 ± 0.2	2.5 ± 0.1	2.7 ± 0.1	2.6 ± 0.2	2.1 ± 0.3	$2.5 \pm 0.5^{1,2,5}$
	R_2 (s^{-1})	7.5 ± 0.7	8.1 ± 0.9	9.0 ± 0.7	9.2 ± 0.5	11 ± 1	$8.9 \pm 1.9^{1,2,5}$
	η	0.53 ± 0.06	0.49 ± 0.16	0.29 ± 0.07	0.29 ± 0.07	0.38 ± 0.16	$0.47 \pm 0.08^{1,2,5}$
	R_2/R_1	2.5 ± 0.3	3.3 ± 0.4	3.4 ± 0.3	3.6 ± 0.3	5.5 ± 0.8	$3.8 \pm 1.6^{1,2,5}$
Man-4′	R_1 (s^{-1})	2.6 ± 0.2	2.7 ± 0.1	2.7 ± 0.1	2.6 ± 0.2	2.8 ± 0.2	$2.7 \pm 0.1^{1,2,5}$
	R_2 (s^{-1})	9.4 ± 0.7	7.9 ± 0.3	9.0 ± 0.7	9.2 ± 0.5	11 ± 1	$9.4 \pm 1.6^{1,2,5}$
	η	0.50 ± 0.06	0.27 ± 0.23	0.29 ± 0.07	0.29 ± 0.07	0.37 ± 0.15	$0.38 \pm 0.12^{1,2,5}$
	R_2/R_1	3.7 ± 0.4	2.9 ± 0.1	3.4 ± 0.3	3.6 ± 0.3	3.9 ± 0.3	$3.5 \pm 0.5^{1,2,5}$
GlcNAc-5,5′	R_1 (s^{-1})	2.4 ± 0.1	2.4 ± 0.2	2.6 ± 0.1	2.5 ± 0.3	2.5 ± 0.2	$2.4 \pm 0.1^{1,2,4}$
	R_2 (s^{-1})	8.2 ± 0.8	5.4 ± 0.8	8.6 ± 1.2	6.4 ± 1.2	9.6 ± 0.6	$6.7 \pm 1.4^{1,2,4}$
	η	0.69 ± 0.25	0.51 ± 0.24	0.24 ± 0.13	0.04 ± 0.25	0.63 ± 0.21	$0.60 \pm 0.13^{1,2}$
	R_2/R_1	3.4 ± 0.4	2.3 ± 0.4	3.3 ± 0.5	2.6 ± 0.6	3.8 ± 0.4	$2.8 \pm 0.6^{1,2,4}$
GlcNAc-5,5′¶	R_1 (s^{-1})	2.4 ± 0.1	2.7 ± 0.1	3.0 ± 0.2	3.0 ± 0.2	2.7 ± 0.1	$2.8 \pm 0.3^{1,3,4,5}$
	R_2 (s^{-1})	8.2 ± 0.8	8.7 ± 0.6	7.2 ± 0.9	8.0 ± 0.8	8.7 ± 0.9	$8.0 \pm 0.6^{1,3,4,5}$
	η	0.69 ± 0.25	0.21 ± 0.13	0.29 ± 0.27	0.54 ± 0.23	0.75 ± 0.08	$0.57 \pm 0.21^{1,3,4,5}$
	R_2/R_1	3.4 ± 0.4	3.3 ± 0.3	2.4 ± 0.3	2.7 ± 0.3	3.3 ± 0.4	$3.0 \pm 0.5^{1,3,4,5}$
GlcNAc-5(t)	R_1 (s^{-1})	2.3 ± 0.1	2.6 ± 0.2	1.9 ± 0.3	2.3 ± 0.3	2.0 ± 0.2	$2.2 \pm 0.4^{2,3,5}$
	R_2 (s^{-1})	7.7 ± 0.9	5.4 ± 0.7	5.6 ± 0.9	6.4 ± 0.4	6.3 ± 0.2	$5.8 \pm 0.5^{2,3,5}$
	η	0.08 ± 0.25	0.77 ± 0.58	0.57 ± 0.31	0.23 ± 0.05	0.85 ± 0.29	$0.73 \pm 0.14^{2,3,5}$
	R_2/R_1	3.3 ± 0.4	2.0 ± 0.3	2.9 ± 0.6	2.8 ± 0.4	3.2 ± 0.3	$2.7 \pm 0.6^{2,3,5}$
Gal-6,6′	R_1 (s^{-1})	2.0 ± 0.5	2.2 ± 0.1	2.3 ± 0.1	2.3 ± 0.1	3.0 ± 0.3	$2.5 \pm 0.7^{1,5}$
	R_2 (s^{-1})	7.2 ± 0.7	5.7 ± 0.3	6.2 ± 0.4	6.9 ± 0.2	6.1 ± 0.5	$6.7 \pm 0.8^{1,5}$
	η	0.17 ± 0.15	0.68 ± 0.08	0.66 ± 0.07	0.64 ± 0.04	0.21 ± 0.17	$0.19 \pm 0.03^{1,5}$
	R_2/R_1	3.6 ± 1.1	2.6 ± 0.2	2.7 ± 0.2	3.0 ± 0.1	2.0 ± 0.3	$2.8 \pm 1.1^{1,5}$
Gal-6,6′¶	R_1 (s^{-1})	2.2 ± 0.3	2.2 ± 0.1	2.3 ± 0.1	2.3 ± 0.1	2.4 ± 0.2	$2.3 \pm 0.1^{1,5}$
	R_2 (s^{-1})	6.4 ± 0.7	5.7 ± 0.3	6.2 ± 0.4	6.9 ± 0.2	4.4 ± 0.7	$5.4 \pm 1.4^{1,5}$
	η	0.64 ± 0.14	0.68 ± 0.08	0.66 ± 0.07	0.64 ± 0.04	0.46 ± 0.11	$0.55 \pm 0.13^{1,5}$
	R_2/R_1	3.0 ± 0.6	2.6 ± 0.2	2.7 ± 0.2	3.0 ± 0.1	1.9 ± 0.4	$2.5 \pm 0.8^{1,5}$
		C4	C5	C6	C7	C8	Average
NeuAc-N,N′	R_1 (s^{-1})	2.4 ± 0.1	2.8 ± 0.3	3.1 ± 0.2	2.5 ± 0.2	2.5 ± 0.1	$2.8 \pm 0.4^{4-6}$
	R_2 (s^{-1})	6.9 ± 0.7	8.2 ± 0.9	5.8 ± 0.6	5.6 ± 0.6	5.2 ± 0.8	$7.0 \pm 1.2^{4-6}$
	η	1.0 ± 0.2	0.90 ± 0.39	0.81 ± 0.16	0.61 ± 0.09	0.47 ± 0.37	$0.90 \pm 0.10^{4-6}$
	R_2/R_1	2.8 ± 0.3	2.9 ± 0.5	1.9 ± 0.3	2.3 ± 0.3	2.1 ± 0.3	$2.5 \pm 0.6^{4-6}$

*The GlcNAc, Gal, and NeuAc residues in the two branches share the same data set because the respective ^{13}C chemical shifts in both branches are degenerate; the same applies to the C3 and C4 of Man-4 and Man-4′.

#See TABLE 1 footnotes for the explanation of how error margins in the various parameters were obtained.

§Numbers in superscript are ring carbons used for calculation of average R_1, R_2, and η values.

¶Indicates the GlcNAc and Gal residues in the branches without the NeuAc residues. The terminal GlcNAc-5(t) residues is located at the $\alpha(1 \rightarrow 3)$ branch of the diantennary oligosaccharide (Lu and Van Halbeek, 1996).

which could not be measured accurately due to severe overlaps, as mentioned previously, such as the C^{α} resonance of Gln-2 in the peptide sequence with pGlu at the NH_2 terminus, may not be reliable either. There is a large simulated standard deviation of the effective internal correlation time τ_e for many of the methine resonances, particularly those with $S^2 > 0.8$. As previously noted by Palmer et al. (Palmer et al., 1991), this observation indicates that the τ_e values for these resonances are not reliable. Therefore, only the τ_e values that are within one standard deviation of the mean are reported in Tables 3 and 4. For the peptide fragment, the average τ_e value is 124 ± 19 ps for the two interior residues Val-10 and Cys-13, and the average τ_e value is 168 ± 18 ps for the four residues in the NH_2- and COOH-terminal regions, namely, Gln-2, Gln-3, Asn-16, and Phe-20. For the carbohydrate moiety, the τ_e values for a number of methine carbons are listed in Table 4. All of the τ_e values reported in Tables 3 and 4 are less than 0.3 ns,

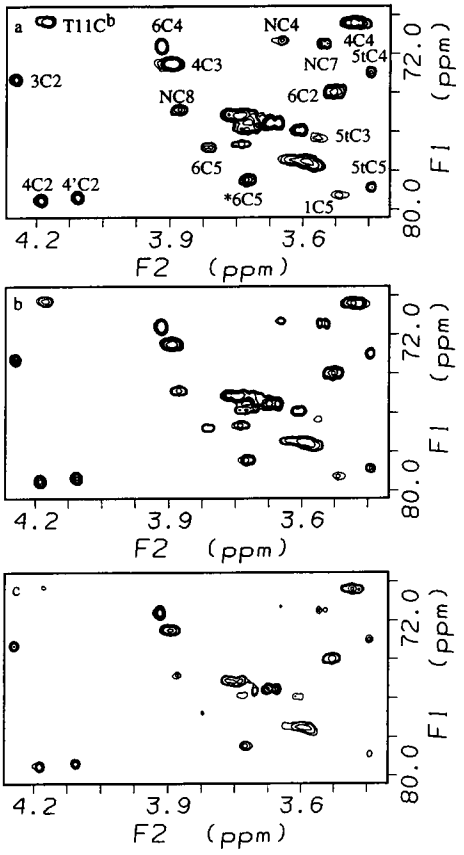

FIGURE 2 HSQC subspectra of Gp21 for longitudinal relaxation rate measurements recorded with different relaxation delays: (*a*) 20 ms; (*b*) 120 ms; and (*c*) 321 ms.

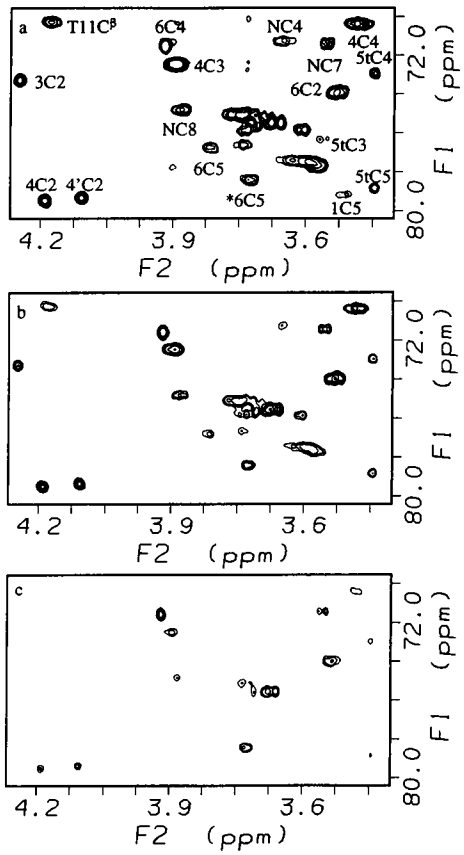

FIGURE 3 HSQC subspectra of Gp21 for transverse relaxation rate measurements recorded with different relaxation delays: (*a*) 11 ms; (*b*) 66 ms; and (*c*) 154 ms.

indicating that the internal motions observed in Gp21 are in the fast internal motion regime and should be completely described by the two model-independent parameters S^2 and τ_e.

Flexibility of the peptide fragment

A graph of the S^2 values for the peptide fragment taken from Table 3 is shown in Fig. 5. As stated previously, the order parameter S^2 ($0 \leq S^2 \leq 1$) is a measure of the spatial restriction of the C-H vector motion, which can be described as the reorientation of the vector with respect to the external magnetic field and is assumed to be independent of the overall rotation of the molecule (Lipari and Szabo, 1982a). $S^2 = 0$ when the vector can reorient freely (isotropic motion); $S^2 = 1$ when the vector reorientation is completely restricted due to, for instance, a steric interaction with the environment. For the peptide fragment, the S^2 values for the three residues in the NH_2-terminal region, Gln-2, Gln-3, and Leu-5, and the S^2 value for Cys-18 in the COOH-terminal region, are the smallest ($S^2 \leq 0.21$) among all amino acid residues, indicating that the C^α-H^α vectors of these residues have a large motional freedom. The S^2 values for the five residues in the COOH-terminal region, Ser-14, Asn-16, Phe-17, Leu-19, and Phe-20, are in the range of 0.33–0.47. These values are similar to the S^2 values for three peptide fragments derived from human transthyretin with each peptide containing 11 amino acid residues (Jarvis and Craik, 1995). The S^2 value (0.77 ± 0.17) for the COOH terminus Arg-21 is unusually large. When a free parameter R_a was added to Eq. 4 (Palmer et al., 1991), which became $R_2' = R_2 + R_a$, to take into account the contribution of conformational exchange that is indicated by the large R_2/R_1 value (see Table 1), the corrected S^2 value was 0.42 ± 0.34. Although the value is comparable with those for Leu-19 and Phe-20, the large deviation for this value makes it difficult to quantify the contribution of conformational exchange to the transverse relaxation rate.

The six amino acid residues around the glycosylation site (Asn-9), Ser-8 to Cys-13, have S^2 values ranging from 0.53 to 0.74, which are larger than those of the rest of the amino acid residues (except for Arg-21). These results indicate that the internal motions in this segment of the peptide backbone are more restricted than in the rest of the peptide. However, NOE data and distance geometry calculations for Gp21 show that no particularly well defined secondary structure was found for this sequence segment or the rest of the peptide (Lu, 1996). The three peptide fragments from human transthyretin have a random coil structure (Jarvis and

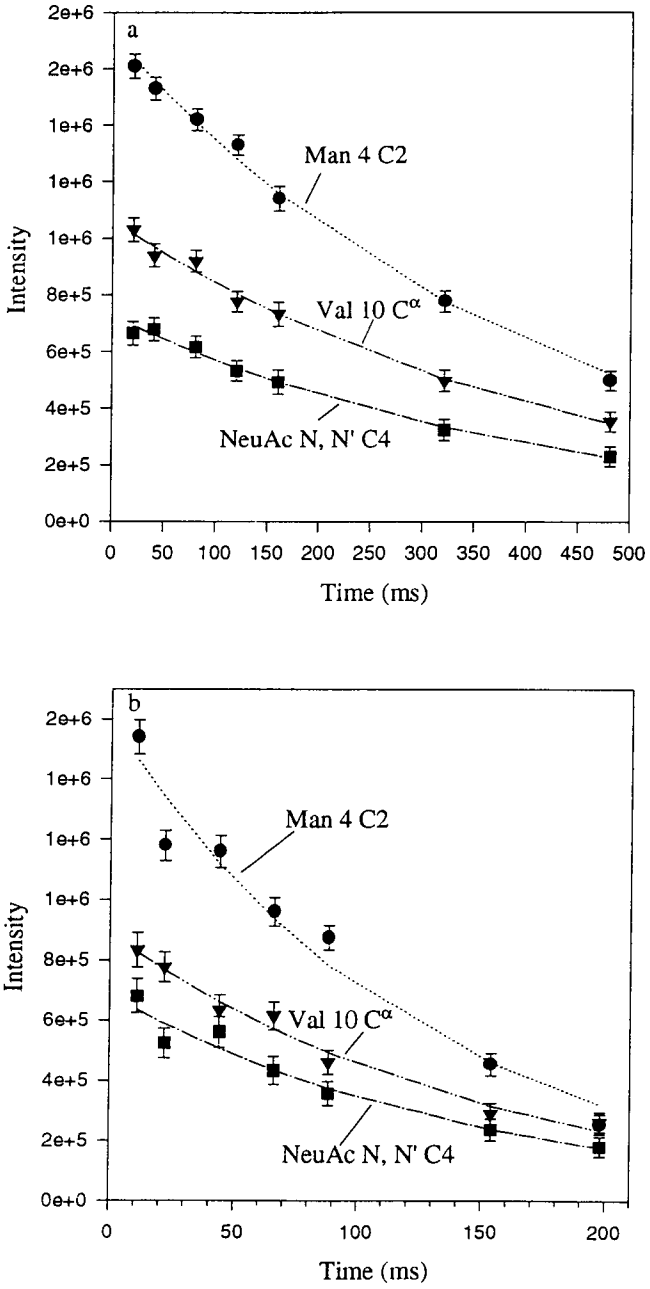

FIGURE 4 The longitudinal (*a*) and transverse (*b*) relaxation decay curves for C^{α} of Asn-9, C2 of Man-4, and C4 of NeuAc-N,N' together with the optimized fits of the peak intensities.

Craik, 1995). They all have quite uniform and small S^2 values (<0.5) throughout the entire sequence. This indicates that the dynamic properties of the peptide fragment of Gp21 are different from those of the peptide fragments from human transthyretin, although neither one of the peptides have a regular secondary structure. This result is not unexpected as there is an *N*-glycan attached to the Gp21 peptide fragment, which may have an effect on the internal motions in the segment of the peptide backbone around the *N*-glycosylation site.

TABLE 3 Model-independent parameters for the methine ^{13}C resonances of the Gp21 peptide fragment

Residue*	$S^{2\#}$	τ_e (ps)	$f(S^2, \tau_e)$
Backbone $^{13}C^{\alpha}$			
Gln-1	1.00 ± 0.00		5.45×10^4
pGlu-1	0.37 ± 0.02	65 ± 10	11.8
Gln-2	0.21 ± 0.06	149 ± 22	0.271
	1.00 ± 0.03		16.7
Gln-3	0.18 ± 0.06	144 ± 34	58.0
His-4	0.61 ± 0.08		0.42
Leu-5	0.16 ± 0.19		6.59
Phe-6	0.47 ± 0.09		0.00
Ser-8	0.74 ± 0.04		0.02
Asn-9	0.68 ± 0.18		6.04
Val-10	0.53 ± 0.05	90 ± 23	1.58
Thr-11	0.65 ± 0.08		1.72
Asp-12	0.73 ± 0.10		0.00
Cys-13	0.55 ± 0.06	157 ± 29	0.92
Ser-14	0.37 ± 0.28	65 ± 10	11.8
Asn-16	0.41 ± 0.06	177 ± 42	0.18
Phe-17	0.47 ± 0.09		0.00
Cys-18	0.16 ± 0.09		6.54
Leu-19	0.33 ± 0.15		0.99
Phe-20	0.33 ± 0.08	200 ± 41	2.16
Arg-21	0.77 ± 0.17		0.69
Side-chain methine ^{13}C			
Thr-11 $^{13}C^{\beta}$	0.46 ± 0.09		9.40

*Each of the two pairs of residues, pGlu-1 and Ser-14 as well as Phe-6 and Phe-17, shares the same data set with the other because their signals are superimposed. The second data set for Gln-2 is due to the presence of pGlu at the NH_2 terminus of a portion of the Gp21 molecules.
#The limits of the S^2 and τ_e values are the standard deviations estimated by Monte Carlo simulations.

There are four side-chain methine carbons in the peptide fragment, but only the S^2 value for Thr-11 C^{β} is reported in Table 3, because the others are not within the observed spectral widths. The S^2 value for Thr-11 C^{β} is 0.46 ± 0.09, which is smaller than 0.65 ± 0.08 for Thr-11 C^{α}, indicating that the internal motion of the C^{β} is less restricted than the C^{α} due to a rotation of the C^{β} about the χ torsion angle. The data are in agreement with previous studies that showed a decrease of S^2 values in an order $C^{\alpha} > C^{\beta} > C^{\gamma}$ (Palmer et al., 1991).

Flexibility of the *N*-linked diantennary oligosaccharide

The average S^2 values for the sugar residues are listed in Table 4. Due to signal degeneracy and overlap for some of the methine carbons, as discussed before, the corresponding S^2 values should be interpreted with caution. Keeping that in mind, average S^2 values were calculated from the selected methine carbons for each sugar residue. A schematic representation of the diantennary oligosaccharide of Gp21 is shown in Fig. 6 together with a summary of the average S^2 values of all of the sugar residues. The average S^2 values for the residues in the pentasaccharide core are in the range of 0.72–0.91, and the highest value (0.91) is obtained for GlcNAc-2 and Man-3. These results indicate that the inter-

TABLE 4 Model-independent parameters for the methine ^{13}C resonances of the Gp21 carbohydrate moiety

Residue*	Parameter‡	C1	C2	C3	C4	C5	Average§
GlcNAc-1	S^2	0.76 ± 0.05	0.78 ± 0.13	0.68 ± 0.08	0.79 ± 0.05	0.57 ± 0.13	0.72 ± 0.09[1–5]
	τ_e (ps)						
	$f(S^2, \tau_e)$	0.00	0.07	0.00	1.93	12.2	
GlcNAc-2	S^2	1.00 ± 0.07	0.84 ± 0.11	1.00 ± 0.08	0.80 ± 0.06	0.76 ± 0.07	0.91 ± 0.11[1–4]
	τ_e (ps)						
	$f(S^2, \tau_e)$	10.7	1.34	15.1	2.19	1.38	
Man-3	S^2	1.00 ± 0.03	1.00 ± 0.00	0.74 ± 0.09	0.82 ± 0.08	1.00 ± 0.13	0.91 ± 0.12[1–5]
	τ_e (ps)						
	$f(S^2, \tau_e)$	40.3	41.9	0.09	0.09	1.40	
Man-4	S^2	0.57 ± 0.07	1.00 ± 0.13	0.83 ± 0.10	0.79 ± 0.04	1.00 ± 0.06	0.86 ± 0.25[1,2,5]
	τ_e (ps)						
	$f(S^2, \tau_e)$	2.93	35.9	2.47	0.59	10.1	
Man-4′	S^2	0.74 ± 0.04	0.60 ± 0.03	0.83 ± 0.10	0.79 ± 0.04	0.91 ± 0.08	0.75 ± 0.16[1,2,5]
	τ_e (ps)		147 ± 25				
	$f(S^2, \tau_e)$	0.22	3.65	2.47	0.59	0.35	
GlcNAc-5,5′	S^2	0.63 ± 0.18	0.45 ± 0.08	1.00 ± 0.00	0.69 ± 0.10	0.76 ± 0.07	0.59 ± 0.13[1,2,4]
	τ_e (ps)		95 ± 51				
	$f(S^2, \tau_e)$	0.15	3.77	18.0	5.03	1.38	
GlcNAc-5,5′#	S^2	0.63 ± 0.18	0.79 ± 0.07	0.51 ± 0.09	0.57 ± 0.08	0.60 ± 0.05	0.58 ± 0.05[1,3,4,5]
	τ_e (ps)					152 ± 34	
	$f(S^2, \tau_e)$	0.15	3.75	2.61	0.37	1.01	
GlcNAc-5(t)	S^2	1.00 ± 0.17	0.31 ± 0.08	0.46 ± 0.07	0.17 ± 0.11	0.48 ± 0.03	0.42 ± 0.09[2,3,5]
	τ_e (ps)		166 ± 50	50 ± 27		61 ± 21	
	$f(S^2, \tau_e)$	38.7	0.36	0.35	40.6	0.25	
Gal-6,6′	S^2	0.45 ± 0.17	0.47 ± 0.03	0.52 ± 0.03	0.55 ± 0.01	0.25 ± 0.09	0.35 ± 0.14[1,5]
	τ_e (ps)		64 ± 15	80 ± 13	76 ± 10		
	$f(S^2, \tau_e)$	12.1	4.61	3.61	3.01	8.81	
Gal-6,6′#	S^2	0.52 ± 0.07	0.47 ± 0.03	0.52 ± 0.03	0.55 ± 0.01	0.50 ± 0.08	0.51 ± 0.01[1,5]
	τ_e (ps)		64 ± 15	80 ± 13	76 ± 10		
	$f(S^2, \tau_e)$	0.215	4.61	3.61	3.01	13.462	
		C4	C5	C6	C7	C8	Average
NeuAc-N,N′	S^2	0.47 ± 0.07	0.59 ± 0.09	0.30 ± 0.08	0.52 ± 0.07	0.35 ± 0.06	0.45 ± 0.15[4–6]
	τ_e (ps)			302 ± 78		143 ± 26	
	$f(S^2, \tau_e)$	0.60	0.28	0.50	8.37	2.90	

*The GlcNAc, Gal, and NeuAc residues in the two branches share the same data set because the respective ^{13}C chemical shifts in both branches are degenerate; the same applies to the C3 and C4 of Man-4 and Man-4′.

‡The limits of the S^2 and τ_e values are the standard deviations estimated by Monte Carlo simulations.

§Numbers in superscript are ring carbons used for calculation of average S^2 values.

#Indicates the GlcNAc and Gal residues in the branches without the NeuAc residues. The terminal GlcNAc-5(t) residue is located at the $\alpha(1\rightarrow3)$ branch of the diantennary oligosaccharide.

nal motions of the C-H vectors in these residues are restricted, especially in GlcNAc-2 and Man-3. This restriction on the internal motions may be responsible for the increased transverse relaxation rate (R_2) values for the glycan core. These results are generally consistent with previous studies that showed motional restriction in the core of an oligosaccharide. For example, an average S^2 value of 1 was obtained for the core residues Glc, Gal, and GalNAc of GD1a (Poppe et al., 1994), and an average S^2 value of 0.91 was obtained for the central mannose residue of a pentasaccharide (Mäler et al., 1996). It should be noted that different S^2 values were obtained for the ring carbons of each of the five residues in the glycan core. Some are close to 1.0, whereas the others are significantly smaller than 1, leading to relatively large deviations for the average S^2 values. Previous ^{13}C relaxation studies (Hajduk et al., 1993) of different monosaccharides showed that average S^2 values for the monosaccharides measured at 20°C were all approximately 0.8, indicating some degrees of motional freedom in the sugar rings. A ring deformation in the form of ring librations, as revealed by MD simulations, was attributed to this motional freedom by Hajduk et al. Therefore, the variability of the S^2 values in each of the five residues in the glycan core suggests that the librations of the ring carbons may have different amplitudes.

The large average S^2 values for the glycan core of Gp21 also suggest that the amplitudes of the fluctuations around the glycosidic linkages in the core are relatively small on the picosecond time scale. The results of the MD simulations with and without explicit water molecules (Balaji et al., 1993; Dauchez et al., 1992; Homans, 1990) about the two glycosidic linkages in Man-3-β1,4-GlcNAc-2-β1,4-GlcNAc-1 show that both linkages are rather rigid. These results are in agreement with our observations on Gp21. MD simulations for the Man-4-α1,3-Man-3 linkage in a fucosylated diantennary oligosaccharide (Dauchez et al., 1992) show that this linkage is also rigid. This is in agreement with our observations. Although there are two populated local minima in the ϕ-ψ map of the potential energy surface of

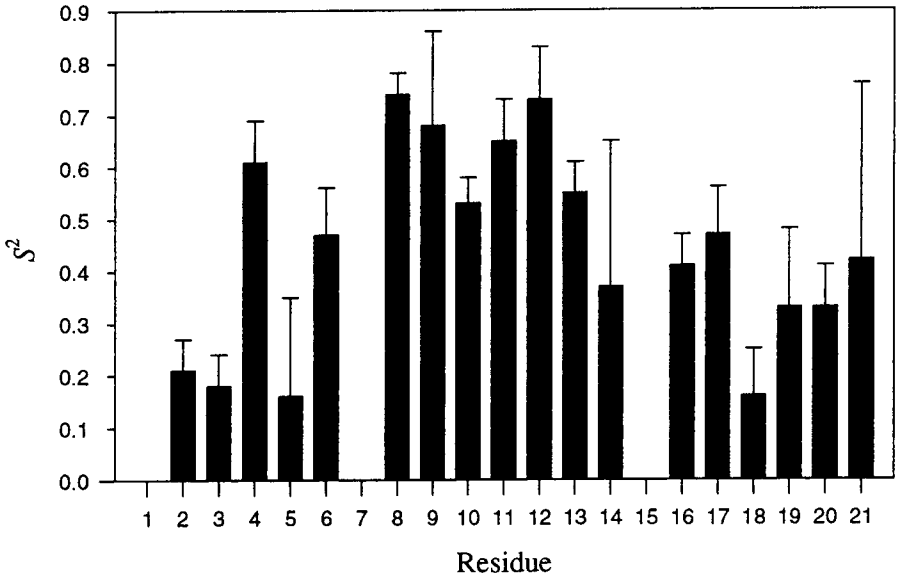

FIGURE 5 Order parameters for methine C^{α}-H^{α} bonds in the Gp21 peptide fragment. The S^2 values, taken from Table 3 except for Arg-21(see text for explanation), are plotted versus the amino acid sequence. The error bars indicate the uncertainties estimated from Monte Carlo simulations. No data are available for Gly-7 and Gly-15 because the C^{α} methylene resonances are suppressed by the INEPT sequence. The data for Gln-1 and Gln-2 are not shown because they are not reliable.

this linkage in the disaccharide (Homans, 1990), the conformational transition between the two local minima is not observed in the 1000-ps MD simulation for a triantennary oligosaccharide (Balaji et al., 1993). This has been explained as being due to the shortness of the simulation period relative to the time scale of the conformational transition. The large R_2 values for the methine carbons in the pentasaccharide core in Gp21 discussed previously suggest that such a conformational exchange may occur for this linkage on a time scale longer than the overall rotational correlation time (2.35 ns).

The average S^2 value for Man-4′ (0.75 ± 0.16) is smaller than that for Man-4 (0.86 ± 0.25), indicating that the mobility of the former residue is less restricted than that of the latter. However, the S^2 values of the corresponding methine carbons in the two residues vary considerably (see Table 4), leading to large standard deviations for the average S^2 values. Therefore, it is difficult to quantify the difference in the mobility between the two residues in terms of the fluctuations around the glycosidic linkages. For the Man-4′-α1,6-Man-3 linkage, the MD simulations of the fucosylated diantennary (Dauchez et al., 1992) and triantennary (Balaji et al., 1993) oligosaccharides showed that there were only small fluctuations of the ϕ, ψ, and ω angles around the corresponding average values despite the fact that this linkage in the disaccharide is more flexible than the others due to the three torsional angles associated with it. These results are in agreement with our observations for the Man-4′-α1,6-Man-3 linkage in Gp21. However, the flexibility of this linkage may be reflected by conformational exchanges that occur on a time scale longer than the overall rotational correlation time, as suggested by the large R_2 values for the ring carbons in Man-4′.

A total of five glycoforms, which vary in the presence of a Gal residue in the α(1 → 3) branch and the NeuAc residues in both branches, have been found in the *N*-linked diantennary oligosaccharide of Gp21 sample used in this work (Lu and Van Halbeek, 1996). The three outer branches which may be found attached to Man-4 and the two outer branches which may be found attached to Man-4′ are sche-

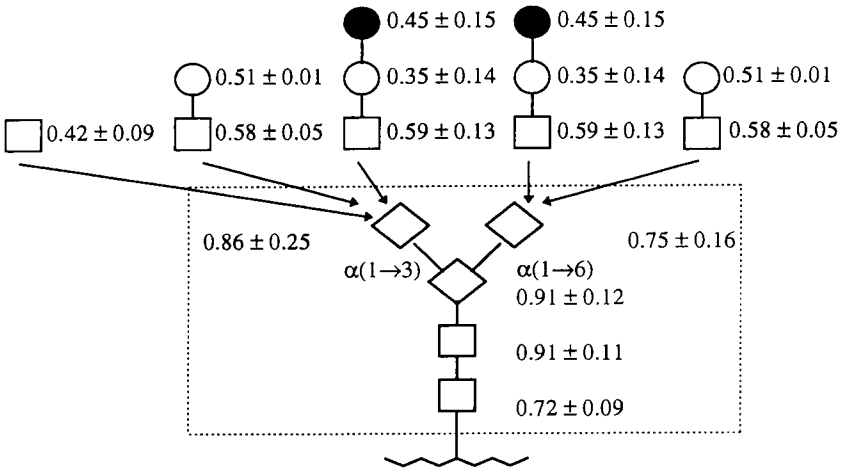

FIGURE 6 A schematic representation of the Gp21 diantennary oligosaccharide. GlcNAc residues are shown as □, Man residues as ◇, Gal residues as ○, and NeuAc residues as ●. The pentasaccharide core is enclosed in the boxed area. Three and two outer chain sequences were found in the α(1 → 3) and α(1 → 6) branches for the Gp21 sample used in this work, respectively. Average order parameter S^2 values are indicated for all sugar residues.

matically depicted in Fig. 6. As the chemical shifts for all of the carbon resonances in the same outer branch sequences, when attached to Man-4 or Man-4′, are degenerate, the respective carbons for the sequences are listed with the same S^2 values, independent of their residue of attachment (see Table 4). This led to the same average S^2 value for the respective residues in the same outer branch sequences at both sites of attachment, as shown in Fig. 6. The general trend observed is that the average S^2 value for the residue at the terminus of any outer branch is smaller than the S^2 values of residues in the interior of the outer branch, with the exception of the interior Gal-6,6′ residues. However, the large deviations associated with the S^2 values make it difficult to quantify the significant differences between them.

The average S^2 values for the residues in the two branches, ranging from 0.35 to 0.59, are smaller than those (0.72–0.91) in the pentasaccharide core, indicating that the internal motions in the two branches are less restricted than in the glycan core. The decrease of the average S^2 values from the core to the branch can be interpreted qualitatively in a simple dynamic model. The GlcNAc-2 and Man-3 residues have the highest average S^2 value (0.91), which means that in approximation the corresponding spectral density functions (Eq. 7) depend on only the overall rotational correlation time τ_m. This amounts to a physical picture in which these two residues are fixed at the origin of a macromolecule's frame and the rest of the sugar residues are attached to this origin through a different number of glycosidic linkages. Thus, if it is assumed that a sugar ring is rigid, the average S^2 values of the sugar residues attached to the macromolecule's frame can be interpreted in a way similar to the method for the S^2 values of various carbons in the long side chain of a lysine residue on a protein surface (Lipari and Szabo, 1982b). If it is assumed that the reorientations about the successive rotation axes in the glycosidic linkages are free and independent, the order parameter of the nth sugar residue ($n = 0$ for GlcNAc-2 and Man-3) is proportional to $(\cos\beta)^{2n}$, where β is the angle between successive rotation axes. Therefore, the average S^2 values decrease as one goes from the core into the two branches, as the number of rotations about the glycosidic linkages increases. These results are consistent with the ^{13}C relaxation studies (Rutherford et al., 1993) of the oligomannose glycan covalently attached to RNAse B, for which the S^2 value (C1, 0.32) of the Man-B residue in the outer branch is smaller than those (C1, 0.46; C2, 0.41) of Man-4′ in the core. Similarly, MD simulations of RNAse B (Woods et al., 1994) and a triantennary oligosaccharide (Balaji et al., 1993) also showed that the sugar residues in the branches of *N*-glycans have more rotational freedom in the glycosidic linkages than those in the glycan core.

CONCLUSIONS

This study has provided a detailed analysis, using the model-free approach, of the dynamics of the *N*-linked diantennary oligosaccharide covalently attached to a polypeptide with 21 amino acid residues. The order parameter S^2 values show that the internal motions are restricted in the segment Ser-8 to Cys-13 containing the *N*-glycosylation site and are less restricted in the NH_2- and COOH-terminal regions. On the other hand, the internal motions are less restricted in the two branches than in the core of the *N*-glycan. We realize that the requirements for applicability of the Lipari-Szabo model-free treatment to the Gp21 molecular system are not rigorously justified by our experimental data. The resulting dynamic model for Gp21, therefore, should be viewed as our initial attempt to analyze the experimental data, bearing in mind the uncertainties introduced by the application of the Lipari-Szabo approach. In the near future, we plan to apply other methods, including spectral density mapping methods (Peng and Wagner, 1992) and extensions to the Lipari-Szabo theory (Clore et al., 1990), to verify the validity of the Gp21 model presented here.

The size of the Gp21 peptide fragment is small relative to the polypeptide of an intact glycoprotein, leading to an overall rotational correlation time (τ_m = 2.35 ns) that is much smaller than that of an intact glycoprotein. In addition, GlcNAc-2 and Man-3 in Gp21 have an average S^2 value of 0.91, which is higher than that for GlcNAc-1. This may not be the case for an intact glycoprotein as the overall rotational correlation time gets longer. It will be interesting to see whether the average S^2 value of GlcNAc-1 becomes larger than those of GlcNAc-2 and Man-3 when the diantennary oligosaccharide is attached to a much larger polypeptide than the Gp21 peptide fragment.

We thank Dr. John Glushka for his assistance in NMR spectroscopy and Drs. John Glushka and William York for critical review of the manuscript. This research is supported by the National Institutes of Health Resource Center grant for Biomedical Complex Carbohydrates (P41-RR05351).

REFERENCES

Abragam, A. 1961. Principles of Nuclear Magnetism. Clarendon Press, Oxford.

Bagley, S., H. Kovacs, J. Kowalewski, and G. Widmalm. 1992. Carbon-13 relaxation study of motional properties of lacto-*N*-neotetraose in solution. *Magn. Reson. Chem.* 30:733–739.

Balaji, P. V., P. K. Qasba, and V. S. R. Rao. 1993. Molecular dynamics simulations of asialoglycoprotein receptor ligands. *Biochemistry.* 32: 12599–12611.

Barbato, G., M. Ikura, L. E. Kay, R. W. Pastor, and A. Bax. 1992. Backbone dynamics of calmodulin studied by ^{15}N relaxation using inverse detected two-dimensional NMR spectroscopy: the central helix is flexible. *Biochemistry.* 31:5269–5278.

Bax A., and D. G. Davis. 1985. MLEV-17-based two-dimensional homonuclear magnetization transfer spectroscopy. *J. Magn. Reson.* 65: 355–360.

Bax, A., and S. S. Pochapsky. 1992. Optimized recording of heteronuclear multidimensional NMR spectra using pulsed field gradients. *J. Magn. Reson.* 99:638–643.

Bodenhausen, G., and D. J. Ruben. 1980. Natural abundance nitrogen-15 NMR by enhanced heteronuclear spectroscopy. *Chem. Phys. Lett.* 69: 185–189.

Brüschweiler, R. 1994. Connections between NMR measurements and theoretical models of structural dynamics of biopolymers in solution. *In*

Nuclear Magnetic Resonance Probes of Molecular Dynamics. R. Tycko, editor. Kluwer Academic Publishers, Norwell, MA. 301–334.

Carver, J. P. 1991. Experimental structure determination of oligosaccharides. *Curr. Opin. Struct. Biol.* 1:716–720.

Clore, G. M., P. C. Driscoll, P. T. Wingfield, and A. M. Gronenborn. 1990. Analysis of the backbone dynamics of interleukin-1β using two-dimensional inverse detected heteronuclear ^{15}N-^{1}H NMR spectroscopy. *Biochemistry.* 29:7387–7401.

Clore, G. M., A. Szabo, A. Bax, L. E. Kay, P. C. Driscoll, and A. M. Gronenborn. 1990. Deviations from the simple two-parameter model-free approach to the interpretation of nitrogen-15 nuclear magnetic relaxation of proteins. *J. Am. Chem. Soc.* 112:4989–4991.

Dauchez, M., J. Mazurier, J. Montreuil, G. Spik, and G. Vergoten. 1992. Molecular dynamics simulations of a monofucosylated biantennary glycan of the *N*-acetyllactosamine type: the human lactotransferrin glycan. *Biochimie.* 74:63–74.

Delsuc, M. A., and J. Y. Lallemand. 1986. Improvement of dynamic range in NMR by oversampling. *J. Magn. Reson.* 69:504–507.

Ejchart, A., and J. Dabrowski. 1992. A ^{13}C T_1 study of conformational and molecular mobility of mono- and difucosyllactoses. *Magn. Reson. Chem.* 30:S115–S124.

Ernst, R. R., G. Bodenhausen, and A. Wokaun. 1987. Principles of Nuclear Magnetic Resonance in One and Two Dimensions. Clarendon Press, Oxford.

Hajduk, P. J., D. A. Horita, and L. E. Lerner. 1993. Picosecond dynamics of simple monosaccharides as probed by NMR and molecular dynamics simulations. *J. Am. Chem. Soc.* 115:9196–9201.

Harris, R. K. 1983. Nuclear Magnetic Resonance Spectroscopy. Pitman Publishing, Marshfield, MA.

Homans, S. W. 1990. A molecular mechanical force field for the conformational analysis of oligosaccharides: comparison of theoretical and crystal structures of Manα1-3 Manβ1-4GlcNAc. *Biochemistry.* 29: 9110–9118.

Homans, S. W., R. A. Dwek, and T. W. Rademacher. 1987. Solution conformations of *N*-linked oligosaccharides. *Biochemistry.* 26: 6571–6578.

Jarvis, J. A., and D. J. Craik. 1995. ^{13}C NMR relaxation studies of molecular motion in peptide fragments from human transthyretin. *J. Magn. Reson.* 107B:95–106.

Kay, L. E., T. L. Jue, B. Bangerter, and P. C. Demou. 1987. Sensitivity enhancement of ^{13}C T_1 measurements via polarization transfer. *J. Magn. Reson.* 73:558–564.

Kay, L. E., L. K. Nicholson, F. Delaglio, A. Bax, and D. A. Torchia. 1992. Pulse sequences for removal of the effects of cross correlation between dipolar and chemical-shift anisotropy relaxation mechanisms on the measurement of heteronuclear T_1 and T_2 values in proteins. *J. Magn. Reson.* 97:359–375.

Kay, L. E., D. A. Torchia, and A. Bax. 1989. Backbone dynamics of proteins as studied by ^{15}N inverse detected heteronuclear NMR spectroscopy: application to staphylococcal nuclease. *Biochemistry.* 28: 8972–8979.

Kowalewski, J. 1989. Nuclear spin relaxation in diamagnetic fluids. I. General aspects and inorganic application. *Annu. Rep. NMR Spectrosc.* 22:307–414.

Lakowicz, J. 1986. Fluorescence studies of structural fluctuations in macromolecules as observed by fluorescence spectroscopy in the time, lifetime, and frequency domains. *Methods Enzymol.* 131:518–567.

Lipari, G., and A. Szabo. 1982a. Model-free approach to the interpretation of nuclear magnetic resonance relaxation in macromolecules. I. Theory and range of validity. *J. Am. Chem. Soc.* 104:4546–4559.

Lipari, G., and A. Szabo. 1982b. Model-free approach to the interpretation of nuclear magnetic resonance relaxation in macromolecules. II. Analysis of experimental results. *J. Am. Chem. Soc.* 104:4559–4570.

Lommerse, J. P. M., L. M. J. Kroon-Batenburg, J. Kroon, J. P. Kamerling, and J. F. G. Vliegenthart. 1995. Conformations and internal mobility of a glycopeptide derived from bromelain using molecular dynamics simulations and NOESY analysis. *J. Biomol. NMR.* 6:79–94.

Lu, J. 1996. Conformational analysis of a 21-amino acid glycopeptide from human serum transferrin: a study by NMR and distance geometry. Ph.D. thesis. The University of Georgia, Athens, GA.

Lu, J., and H. van Halbeek. 1996. Complete ^{1}H and ^{13}C resonance assignments of a 21-amino acid glycopeptide prepared from human serum transferrin. *Carbohydr. Res.* In press.

Mäler, L., G. Widmalm, and J. Kowalewski. 1996. Motional properties of a pentasaccharide containing a 2,6-branched mannose residue as studied by ^{13}C nuclear spin relaxation. *J. Biomol. NMR.* 7:1–7.

Marion, D., and K. Wüthrich. 1983. Application of phase sensitive two-dimensional correlated spectroscopy (COSY) for measurements of ^{1}H-^{1}H spin-spin coupling constants in proteins. *Biochem. Biophys. Res. Commun.* 113:967–974.

Meyer, B. 1990. Conformational aspects of oligosaccharides. *Top. Curr. Chem.* 154:141–208.

Neuhaus, D., and M. Williamson. 1989. The Nuclear Overhauser Effect in Structural and Conformational Analysis. VCH Publishers, New York.

Palmer III, A. G., M. Rance, and P. E. Wright. 1991. Intramolecular motions of a zinc finger DNA-binding domain from Xfin characterized by proton-detected natural abundance ^{13}C heteronuclear NMR spectroscopy. *J. Am. Chem. Soc.* 113:4371–4380.

Peng, J. W., and G. Wagner. 1992. Mapping of spectral density functions using heteronuclear NMR relaxation measurements. *J. Magn. Reson.* 98:308–332.

Peng, J. W., and G. Wagner. 1994. Investigation of protein motions via relaxation measurements. *Methods Enzymol.* 239:563–596.

Poppe, L., H. van Halbeek, D. Acquotti, and S. Sonnino. 1994. Carbohydrate dynamics at a micellar surface: GD1a headgroup transformations revealed by NMR spectroscopy. *Biophys. J.* 66:1642–1652.

Press, W. H., S. A. Teukolsky, W. T. Vetterling, and B. P. Flannery. 1992. Numerical Recipes in C. Cambridge University Press, Cambridge.

Rutherford, T. J., J. Partridge, C. T. Weller, and S. W. Homans. 1993. Characterization of the extent of internal motions in oligosaccharides. *Biochemistry.* 32:12715–12724.

Shaka, A. J., P. B. Baker, and R. Freeman. 1985. Computer-optimized decoupling scheme for wideband applications and low-level operation. *J. Magn. Reson.* 64:547–552.

Sklenar, V., D. Torchia, and A. Bax. 1987. Measurement of carbon-13 longitudinal relaxation using ^{1}H detection. *J. Magn. Reson.* 73:375–379.

Van Halbeek, H. 1994. NMR developments in structural studies of carbohydrates and their complexes. *Curr. Opin. Struct. Biol.* 4:697–709.

Woods, R. J., C. J. Edge, and R. A. Dwek. 1994. Protein surface oligosaccharides and protein function. *Nature Struct. Biol.* 1:499–501.

Wyss, D. F., J. S. Choi, J. Li, M. H. Knoppers, K. J. Willis, A. R. N. Arulanandam, A. Smolyar, E. L. Reinherz, and G. Wagner. 1995. Conformation and function of the *N*-linked glycan in the adhesion domain of human CD2. *Science.* 269:1273–1278.